Multiple magnetic ordering phenomena in multiferroic *o*-$HoMnO_3$

Y. W. Windsor,[1,2] M. Ramakrishnan,[1] L. Rettig,[1,2] A. Alberca,[1] T. Lippert,[3,4] C. W. Schneider,[3] and U. Staub[1]

[1]*Swiss Light Source, Paul Scherrer Institute, 5232 Villigen PSI, Switzerland*

[2]*Department of Physical Chemistry, Fritz-Haber-Institute of the Max Planck Society, Faradayweg 4-6, Berlin 14915, Germany*

[3]*Laboratory for Multiscale Materials Experiments, Paul Scherrer Institute, 5232 Villigen PSI, Switzerland*

[4]*Department of Chemistry and Applied Biosciences, Laboratory of Inorganic Chemistry, ETH Zurich, Switzerland*

(Received 3 August 2020; revised 9 November 2020; accepted 30 November 2020; published 18 December 2020)

Orthorhombic $HoMnO_3$ is a multiferroic in which Mn antiferromagnetic order induces ferroelectricity. A second transition occurs within the multiferroic phase, in which a strong enhancement of the ferroelectric polarization occurs concomitantly to antiferromagnetic ordering of Ho $4f$ magnetic moments. Using the element selectivity of resonant x-ray diffraction, we study the magnetic order of the Mn $3d$ and Ho $4f$ moments. We explicitly show that the Mn magnetic order is affected by the Ho $4f$ magnetic ordering transition. Based on the azimuthal dependence of the $(0\,q\,0)$ and $(0\,1{-}q\,0)$ magnetic reflections, we suggest that the Ho $4f$ order resembles an *ac* cycloid. Using nonresonant diffraction, we show that the magnetically induced polar lattice distortion is unaffected by the Ho ordering, suggesting a mechanism through which the Ho order affects ferroelectric polarization without affecting the lattice in the same manner as the Mn order.

DOI: 10.1103/PhysRevB.102.214423

I. INTRODUCTION

Perovskite manganites of the o-$RMnO_3$ family (*o* is short for orthorhombic, *R* denotes a rare-earth lanthanide or Y) have been the subject of significant attention for over a decade, owing mostly to their magnetically induced ferroelectricity (type-II multiferroic behavior), which occurs for *R* ions heavier (smaller) than Gd [1] (i.e., Tb-Lu and Y). All materials in this family exhibit antiferromagnetic (AF) orders of Mn moments that can be described by the same parametrized ordering wave vector $\mathbf{Q} = (0\,q\,1)$, with different values of q (using *Pbnm* notation). The Mn magnetic ordering pattern varies between these materials. For example, $TbMnO_3$ acquires a *bc* cycloidal AF structure ($q \approx 0.27$) [2], while for $LuMnO_3$ an *E*-type AF structure is known to occur ($q = 0.5$) [3]. These AF orders induce a spontaneous ferroelectric polarization $\boldsymbol{P}$. The magnitude of the ferroelectric polarization $\boldsymbol{P}$ induced by these AF orders depends on the ordering pattern: the AF cycloids are accompanied by $P \approx 500\ \mu C/m^2$, while for the *E*-type AF a much larger value of $P \approx 5000\ \mu C/m^2$ is expected [1]. In all cases the inverse Dzyaloshinskii-Moriya interaction contributes to P, but enlarged P values are understood to arise due to symmetric exchange striction [4,5].

Regardless of the exact Mn magnetic ordering motif, it is well-established that the ferroelectricity in these materials is induced by the Mn AF order, and not by that of the *R* ions. An exception to this is the case of *o*-$HoMnO_3$. Here an additional magnetic phase transition occurs well within the multiferroic phase, below which P rises sharply by an order of magnitude. This behavior is illustrated in Fig. 1. Neutron diffraction studies have associated this transition with an AF ordering of the Ho^{3+} $4f$ moments [6]. Similar spontaneous *R*-ion magnetic order has been reported for other *o*-$RMnO_3$ materials, but at very low temperatures (e.g., for Tb, Dy, and Tm this occurs at 7, 5, and 4 K, respectively [7,8]). However, such a strong enhancement of P has not been reported for other *R* ions.

An early study of *o*-$HoMnO_3$ suggested that Mn moments form an *E*-type AF order, implying a commensurate $q = 0.5$ [11]. Later studies indicated that an incommensurate AF order occurs with $q \approx 0.41$ [6,9]. Nevertheless from the experimental phase diagram [1,12] it is clear that $HoMnO_3$ is at the border between *E*-type AF and cycloidal AF structures, so variations in sample preparation could explain the difference in magnetic structure. Indeed more recent work by Shimamoto *et al.* has shown that epitaxial strain can "push" $HoMnO_3$ towards *E*-type AF behavior [13].

Upon cooling, the Mn moments in multiferroic *o*-$RMnO_3$ order in a sinusoidal AF structure below T_N. Upon further cooling they acquire a second magnetic component below T_c, producing the full Mn AF order, which induces a polar structural distortion and ferroelectricity (for the case of $R = Ho$, $T_N \approx 40$ K, and $T_c \approx 35$ K). For heavy *R* ions the difference between T_c and T_N is only a few K, so they are often not explicitly distinguished in the literature. The Ho ordering transition, below which P rises sharply, occurs at a lower temperature of $T_{Ho1} \approx 14.5$ K [9]. The mechanism behind this enhancement is not known, but one could expect a further distortion of the lattice.

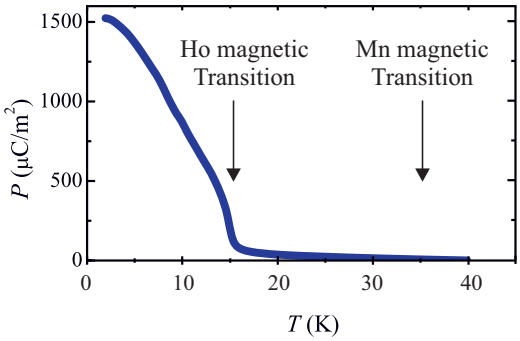

FIG. 1. Polarization dependence of a crystal of $HoMnO_3$, adapted from Ref. [9]. Similar behavior is shown for a polycrystalline sample in Ref. [10].

The study of $HoMnO_3$ and other heavy-R perovskite materials from this family has been limited due to the absence of single crystals. To date only one case of single crystalline $HoMnO_3$ has been reported [9]. In this work we study the magnetic and structural orders of o-$HoMnO_3$ using x-ray diffraction techniques on *thick* single-crystalline films. Using resonant x-ray diffraction (RXD) we observe the AF orders, and identify a strong coupling between the Mn $3d$ and the Ho $4f$ moments, specifically around the 14.5 K transition. Nonresonant diffraction is used to follow symmetry-forbidden Bragg reflections, the appearance of which herald the lowering of crystal symmetry that is associated with the occurrence of ferroelectricity. RXD is also used to provide a detailed account of the evolution of the Ho moments, which are shown to be strongly affected by three magnetic transitions.

II. EXPERIMENT

o-$HoMnO_3$ films were grown on $NdGaO_3$ [010] substrates (Crystec Co. Ltd.) by pulsed laser deposition. Pulsed beams from a KrF excimer laser ($\lambda = 248$ nm, $\tau = 25$ ns) were imaged onto a stoichiometric hexagonal $HoMnO_3$ ceramic target with a fluence of 2.3–2.7 J cm^{-2} at a repetition rate of 2 Hz in a N_2O partial pressure of 0.30 mbar. The target-substrate distance was fixed at 37 mm and the substrate was heated to 780 °C during the film growth. The crystal structure and quality of the as-deposited films were investigated using Cu-$K\alpha$ x-ray diffraction. Since thin films are known to acquire different magnetic order than bulk samples [13], all results are from thick films (120, 240 nm, see Appendix A) that exhibit the magnetic transitions described in the following.

Resonant x-ray diffraction experiments (RXD) were conducted using the RESOXS UHV diffraction end station [14] at the SIM beam line [15] of the Swiss Light Source (SLS). Photon energies used correspond to the Mn $L_{2,3}$ absorption edges ($2p \rightarrow 3d$, ~643 and ~652 eV) and to the Ho $M_{4,5}$ absorption edges ($3d \rightarrow 4f$, ~1390 and ~1350 eV). The large resonant enhancement of magnetic diffraction at these edges renders the collected signals solely sensitive to the resonant ion. Linearly polarized incident light was used, with either π or σ polarization (electric field in the scattering plane, or perpendicular to it, respectively). Scattered intensities were collected using an IRD AXUV100 photodiode. Azimuthal rotation of the sample around the momentum transfer vector

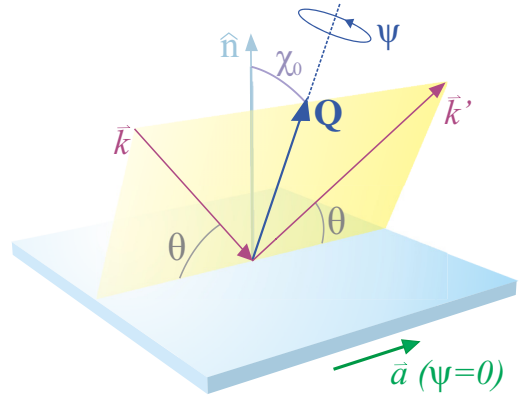

FIG. 2. Experimental geometry of the RXD experiment. The scattering plane contains the momentum transfer $\boldsymbol{Q}$ and the directions of the incoming and outgoing beam, $\vec{k}$ and $\vec{k}'$, respectively. θ is the Bragg angle and χ_0 is the angle between $\boldsymbol{Q}$ and the film surface normal $\hat{n}$. Ψ is the angle of azimuthal sample rotation around the $\boldsymbol{Q}$ direction.

$\boldsymbol{Q}$ was conducted using a mechanical arm to a precision of $\pm 3°$ (see experimental geometry in Fig. 2). We define the azimuthal angle Ψ as zero when the crystallographic $\hat{a}$ axis is in the scattering plane. Nonresonant x-ray diffraction (XRD) was conducted using a 3+2 diffractometer at the Surface Diffraction end station of the Materials Science beam line of the SLS [16]. The incoming photons had an energy of 10 keV, and were linearly polarized. Diffracted intensities were collected using a Pilatus 100-K detector [17] mounted on the detector arm. In both experiments, samples were mounted on the cold head of a Janis ST-400 flow cryostat and cooled to temperatures as low as 9 K.

III. RESULTS

A. RXD study of magnetic order

Figure 3(a) presents scans taken along the [010] direction at 10 K, using photon energies near the Mn L_3 and the Ho M_5 edges. In both cases a magnetic reflection is observed at $(0\,q\,0)$, with $q \approx 0.41$ (r.l.u.). This value coincides with that found in bulk studies, confirming that our thick films are bulklike, and not significantly strained. An additional $(0\,1{-}q\,0)$ magnetic reflection is observed at the Ho edge, which is absent at the Mn edge. A (0 1 0) reflection due to Templeton-Templeton scattering is also observed at resonance (not shown), which is related to $4f$ quadrupole ordering, and also persists in the paramagnetic phase ($T > T_N$). This is analogous to the (1 0 0) reflection observed for o-$TmMnO_3$ [18]. The inset presents the energy dependence of the $(0\,q\,0)$ reflection around the Mn L edges at 9 and 18 K (above and below $T_{\mathrm{Ho1}} = 14.5$ K). The data are normalized at the peaks of the L_3 edge, highlighting a shift in spectral weight between the two edges (see colored region at L_2).

Figures 3(b) and 3(c) present the temperature dependence of these signals, measured at the Mn L_3 and Ho M_5 edges, respectively. For easy comparison, the data were collected in the same experiment and with the same geometry, using π polarized light at $\Psi = 0°$. The $(0\,q\,0)$ reflection appears at

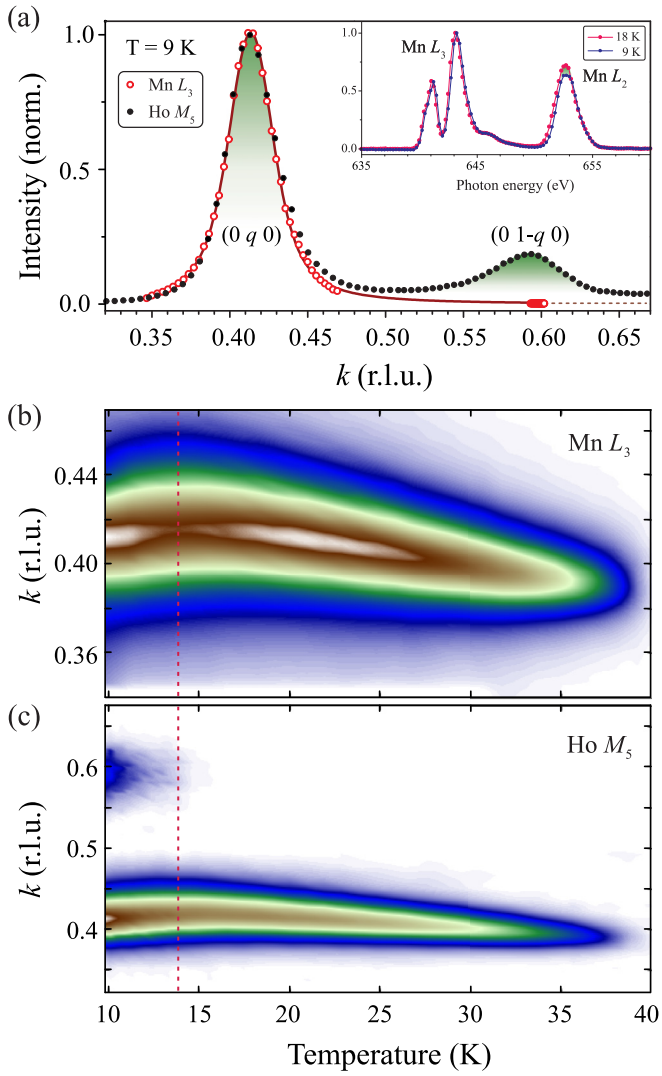

FIG. 3. (a) Scans along (0 k 0) taken at 9 K using photons energies corresponding to the Mn L_3 and the Ho M_5 edges (642.5 and 1349.75 eV, respectively). The (0 q 0) reflection is observed at both energies, and the (0 1−q 0) is observed only for Ho. A dashed line marks the Mn curve beyond the Ewald sphere. Inset: energy dependence of the (0 q 0) reflection at the Mn L edges at 10 and at 18 K (above and below T_{Ho1}), with intensities normalized to the peak of the L_3. Panels (b) and (c) present a temperature dependence of scans along (0 k 0), measured at the Mn L_3 and Ho M_5 edges, respectively. A dashed line is drawn at T_{Ho1}. All data were taken with π polarized light and $\Psi = 0^\circ$. The reflectivity background was removed for clarity.

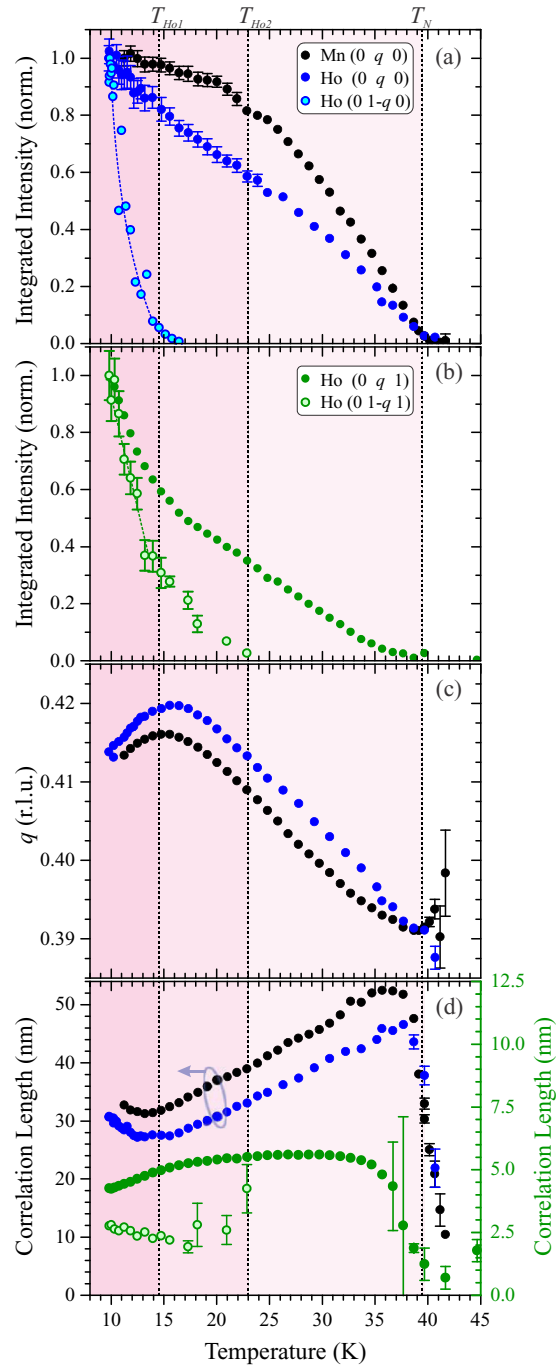

FIG. 4. Temperature dependencies. (a) The integrated intensity from specular magnetic reflections measured at the Mn and Ho edges. (b) The integrated intensity from off-specular the reflections observed only at the Ho M_5 edge (1348 eV). (c) Peak position of the (0 q 0) reflection measured at both edges. (d) Correlation lengths calculated from the widths of the magnetic reflections. Values for the off-specular reflections are given on the right hand axis. All data were collected with π polarized incoming light at $\Psi = 0^\circ$.

both edges below $T_N \approx 39$ K. The T_{Ho1} transition is marked by a dashed red line. Clear signatures of this transition are observed at both resonances: at the Mn edge a dip in the (0 q 0) intensity occurs, and upon further cooling this reflection's intensity at the Ho edge rapidly increases. Most importantly, below T_{Ho1} the (0 1−q 0) reflection appears at the Ho edge. To better quantify these observations, Fig. 4(a) presents the integrated intensity of these reflections as functions of temperature. The Mn integrated intensity increases rapidly upon cooling below T_N, but flattens out below the Ho transitions. The Ho integrated intensities grow upon cooling below these transitions.

The higher energy of the Ho M_5 edge enlarges the Ewald sphere, which permits access to additional magnetic reflections. Figure 4(b) presents the integrated intensity of the

$(0\,q\,1)$ and $(0\,1{-}q\,1)$ magnetic reflections, also measured using π polarized light at $\Psi = 0°$. Both reflections intensify rapidly below T_{Ho1}. However, while the $(0\,q\,1)$ reflection appears below $T_{\mathrm{N}} = 39$ K, the $(0\,1{-}q\,1)$ appears below a third magnetic transition: $T_{\mathrm{Ho2}} = 23$ K. This transition was observed in Ref. [11], but with $q = \frac{1}{2}$. At 9 K the integrated intensity ratio $(0\,1{-}q\,1)/(0\,q\,1)$ is 0.48 or 0.66 for π and σ incoming light, respectively.

Figure 4(c) presents the temperature dependence of q, obtained from the position of the $(0\,q\,0)$ reflection in Figs. 3(b) and 3(c). q varies smoothly with temperature, and peaks around T_{Ho1}. The q values from the Ho and Mn data sets closely follow each other, demonstrating that the Ho and Mn moments are coupled throughout the observed temperature range. The apparent shift between them is due to the difference in refractive index between the two energies, as similarly reported for o-$TmMnO_3$ in Ref. [19]. This wave-vector relation has been noted as an indicator for stronger R-Mn coupling than in o-$TbMnO_3$ and o-$DyMnO_3$ [20]. Figure 4(d) presents the correlation length of $(0\,q\,0)$ at the Ho and Mn edges, defined as $2/\Gamma$ of the reflection (Γ is the full width at half maximum). A continuous reduction occurs upon cooling between T_N and T_{Ho1} (i.e., peak widening), indicating increasing local disorder, such as due to antiferromagnetic domain walls. A change in this trend is observed at both edges at T_{Ho1} and slightly below T_N. The changes in the Mn data around T_{Ho1} occur ∼1.5 K lower than the changes in the Ho data. This systematic difference is not clear around T_N. The correlations lengths of the off-specular reflections are also shown. These do not follow the same trend as $(0\,q\,0)$, and are likely limited by the reduced probe depth of these reflections.

The azimuthal angle dependence of the specular reflections' intensity was also collected. Figures 5(a) and 5(b) present the $(0\,q\,0)$ reflection at the Mn and Ho edges, respectively, using π and σ incoming light at 18 K (between T_{Ho1} and T_{Ho2}). Data are normalized to the sum $(I_\pi + I_\sigma)$ to eliminate extrinsic artifacts. The solid lines represent calculations of the expected signal when only c axis moments contribute to it (detailed in previous works [19,21]). This is in agreement with both the Mn and the Ho data. Because the Ho ions are in the 4c position of the unit cell, small contributions to intensity could indeed occur if Ho moment components exist that are perpendicular to the c axis (see Appendix B). Last, Figure 5(c) presents the azimuthal dependence of $(0\,1{-}q\,0)$ at ∼10 K. Large uncertainties are apparent because this reflection appears only below T_{Ho1}, and is therefore weak, as this is near the lower limit of the experimental cooling range. Nevertheless, the azimuthal pattern clearly exhibits a $\pi/2$ phase shift compared to the $(0\,q\,0)$ intensities in Figs. 5(a) and 5(b). Last, we note that all orders probed in Fig. 5 exhibit an azimuthal dependence I_σ that reaches 0, suggesting that no b-axis moment component is present, as this would cause a nonzero constant offset [22].

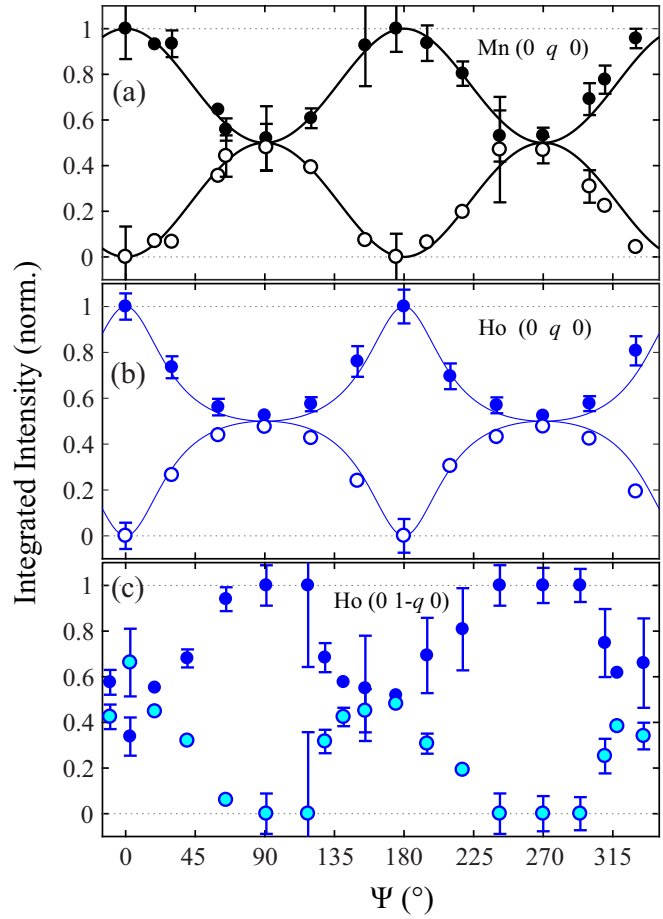

FIG. 5. Azimuthal angle dependence of specular magnetic reflections: (a) the $(0\,q\,0)$ at the Mn L_3 edge (18 K); (b) the $(0\,q\,0)$ at the Ho M_5 edge (18 K; very similar results were obtained at ∼10 K); (c) the $(0\,1{-}q\,0)$ at the Ho M_5 edge (∼10 K). Dark and light markers represent π and σ polarized incoming light, respectively. All data are normalized to the sum of π and σ intensities. Solid lines are calculations of c axis magnetic moments (see Appendix B).

B. Crystal lattice distortion

Several studies on o-$R$$MnO_3$ multiferroics have reported a structural distortion within the multiferroic phase [19,21,23] (below T_c), which is indicative of a lowering of crystal symmetry from *Pbnm*. One study has suggested that the low temperature symmetry is $P2_1nm$ (space group 31), which is polar [24]. This agrees with polarization along the a axis (as reported for a thick film in Ref. [13]), but not along the c axis, which has been reported for single crystal o-$HoMnO_3$ [9]. The distortion is typically observed using XRD, by studying structural reflections that are forbidden by the high temperature space group. Figure 6 presents the integrated intensity of (033) and (022) as functions of temperature. The (033) reflection is forbidden by *Pbnm* but could be allowed in a lower symmetry space group (such as $P2_1nm$), while (022) is allowed, making it orders of magnitude more intense, as the structural distortion is small. The (033) is therefore a measure of the polar structural distortion, although it does not necessarily correlate to the polarization magnitude itself. This would depend on the low temperature space group and corresponding polarization direction, both of which we do not resolve here. In Fig. 6 the magnetically induced polar distortion is clearly apparent, as the intensity of (033) increases sharply below T_c. A contribution to intensity from the (033) remains above T_c, which is the same magnitude as the intensity caused

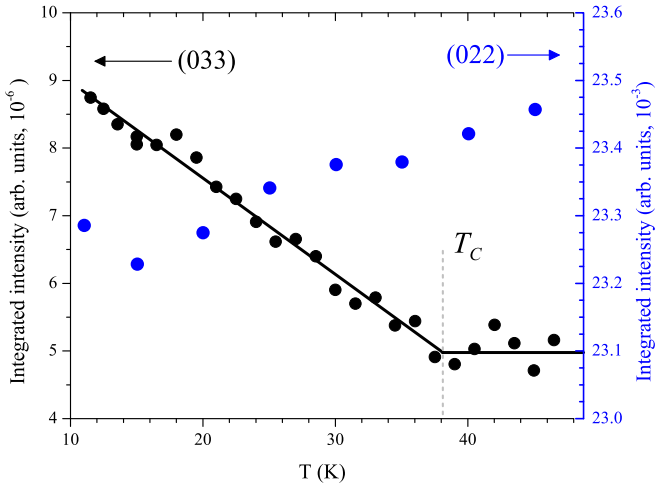

FIG. 6. Temperature dependence of the integrated intensity of structural reflections, taken from a 240-nm-thick [010]-oriented film. The (033) reflection corresponds to the left axis, the (022) corresponds to the right axis. Integrated intensity values are directly comparable, and all diffracted intensities were corrected for the polarization factor and for variations in the scattering volume due to sample rotation.

by the magnetically induced distortion. As the magnetically induced distortion is known to be very small, we attribute this addition to a very small strain-induced distortion in the film that is independent of temperature. Notably no clear jump is observed below $T_{\mathrm{Ho1}} \approx 14.5\,\mathrm{K}$. Other *Pbnm*-forbidden reflections were also studied, and none exhibited a signature of T_{Ho1}.

IV. DISCUSSION

The most prominent observation in these results is that the Mn AF order is affected by the Ho ordering transition associated with $\boldsymbol{P}$ enhancement (T_{Ho1}). A certain level of coupling is to be expected between the Mn and Ho moments. Through dipolar interactions, the Mn order should induce an AF order with the same periodicity onto the paramagnetic Ho moments, as previously shown for $NdNiO_3$ and *o*-$TmMnO_3$ [19,25]. This is directly evident from the temperature dependence of q in Fig. 4(c). However, unlike these previous reports, we observe clear signatures that Ho $4f$ order affects the Mn $3d$ moments as well. This is primarily noticeable at the T_{Ho1} transition, in Figs. 3 and 4. A weak effect is possibly also observed on the Mn intensity around $T_{\mathrm{Ho2}} \approx 23\,\mathrm{K}$.

For clarity, we now limit ourselves to distinguishing between moment components along the c axis (m_c) and moments in the ab plane (m_{ab}). For the Mn ions, the main magnetic order parameter is described by a $(0\,q\,1)$ wave vector. This is the order parameter responsible for the lattice distortion, and it is coupled to a second order parameter, described by $(0\,q\,0)$, which is the order we observe at the Mn L_3 edge. The commonly accepted scenario is that the $(0\,q\,1)$ order is primarily caused by the modulation of the Mn m_{ab}, while the $(0\,q\,0)$ one is caused by the modulation of the Mn m_c. The azimuthal dependence of the Mn $(0\,q\,0)$ reflection is in good agreement with this scenario, and is well-described by the calculation in Fig. 5(a). Also, for a *bc* cycloid the azimuthal dependence from incoming σ-polarized light is strictly never 0, unlike in the present case. A further consideration is that Ref. [19] demonstrated that the order induced on the rare-earth $4f$ sites would exhibit a significantly different azimuthal dependence than the one observed. These considerations rule out a *bc* cycloid as the main Mn AF motif (as in the case of $TbMnO_3$), but could agree with an *ab* cycloid (as in the case of $DyMnO_3$) or a modulated *E*-type (as suggested in Refs. [19,21,26]). The order induced below T_N by the Mn on the paramagnetic Ho moments therefore contains only moment components along the c axis [19]. At the Ho edge, the $(0\,q\,0)$ and $(0\,q\,1)$ reflections appear directly below T_N, indicating that they are sensitive to the induced order. The $k = 1 - q$ type reflections do not appear at the Mn L edges, and at the Ho edge they appear, but at temperatures lower than T_N. These reflections therefore serve as indicators of additional magnetic transitions that the Ho moments undergo independently, T_{Ho1} and T_{Ho2}. They suggest a more complicated structure than that of the Mn, such as the one described in Ref. [6], and are sensitive to this order, not to the induced order from the Mn.

The sensitivity of these reflections to different moment components is described in detail in Appendix B: $(0\,k\,1)$-type reflections are primarily sensitive to m_{ab}, while $(0\ k\ 0)$ type are primarily sensitive to m_c. The appearance of $(0\,1{-}q\,1)$ at $T_{\mathrm{Ho2}} = 23\,\mathrm{K}$ therefore suggests an ordering of the Ho m_{ab}. Indeed T_{Ho2} bares no clear signature on the $(0\,q\,0)$ signal at the Ho edge [Fig. 4(a)], suggesting that the order parameter associated with T_{Ho2} is a weak contribution to this reflection (at $\Psi = 0^\circ$). The appearance of $(0\,1{-}q\,0)$ at $T_{\mathrm{Ho1}} = 14.5\,\mathrm{K}$ is expected to indicate independent ordering of the Ho m_c components. However, the dominant contribution to the Ψ dependence of $(0\,1{-}q\,0)$ in Fig. 5(c) has a $\pi/2$ phase shift to the c-axis components in Figs. 5(a) and 5(b). This suggests that despite the preferred sensitivity to m_c, the dominant contribution to (0 1-q 0) is an a-axis component. This agrees with the sharp intensity rise observed below T_{Ho1} in the $(0\,q\,1)$ and $(0\,1{-}q\,1)$ reflections [Fig. 4(b)]. An equivalent phase shift was observed in $TbMnO_3$, when measured at the Tb L edges [27,28]. This strongly suggests that the Ho order below T_{Ho1} is an *ac*-cycloid-like arrangement. The evolution of the Ho moments with T is best described by dividing the temperatures below T_N into three ranges, as done in Fig. 4. Since the enhancement of $\boldsymbol{P}$ occurs only below T_{Ho1} (Fig. 1), we associate it with the independent order of the Ho m_a. Note that we do not draw a clear conclusion for m_c below T_{Ho1}, but suggest that it is ordered.

The mechanism through which the ordered Ho moment relates to the large P enhancement is still unclear. The *Pbnm*-forbidden reflection (033) is sensitive to the magnetically induced lattice distortion, but showed no change in trend below T_{Ho1}. The integrated intensity of such reflections has been previously shown to scale linearly with that of $(0\,q\,0)$ at the Mn edge [21]. This occurs because both are coupled to the main Mn $(0\,q\,1)$ order parameter, as was reported for *o*-$LuMnO_3$ in which R ion ordering does not occur. From Figs. 4 and 6 it is clear that such a relation with (033) can only hold in the range $T_{\mathrm{Ho2}} < T < T_{\mathrm{N}}$. Below this range

the integrated intensity of the Mn $(0\,q\,0)$ remains mostly constant with cooling (albeit with increasing local disorder), while the (033) continues to grow linearly. This suggests that the Mn m_c [the $(0\,q\,0)$ order] is not coupled to the lattice distortion occurring due to the influence of the Ho order.

Since the primary Mn order parameter $(0\,q\,1)$ is directly coupled to the Ho m_c moments through dipolar interactions [19], a change in the Ho m_c moment (such as *ac* cycloidal order) could affect or enhance the lattice distortion. Such an enhancement effect of the Ho on the Mn-induced polarization is also supported by results from $DyMnO_3$ and $TbMnO_3$ [7,8,20]. In these studies, the *R* ions order, and cause a minor increase in $\boldsymbol{P}$. Furthermore, the *R* ions order with a different q than the Mn ions (Tb and Dy order with $q = 0.415$ and 0.5, compared to Mn with 0.27 and 0.36, respectively). This is unlike $HoMnO_3$, in which Ho and Mn keep the same q value, indicating a stronger coupling between the two orders. Furthermore, as the Mn order is not a *bc* cycloid (as seen in Fig. 5(a), and according to Ref. [19]), one could expect a different response of the Mn-induced polarization, which involves symmetric exchange striction in addition to inverse Dzyaloshinskii-Moriya interaction. However, the absence of any signature of T_{Ho1} in the (033) signal (Fig. 6) indicates that the $\boldsymbol{P}$ enhancement (Fig. 1) does not involve this lattice distortion. This could occur if the additional $\boldsymbol{P}$ contribution is a purely electronic contribution, which does not involve a further distortion of the lattice. Another consideration is that the (033) is a measure for the strength of the ferroelectric phase, because it appears due to the symmetry lowering caused by the Mn order. However, it does not measure the ferroelectric lattice distortion itself, and may not be coupled to the additional distortion created by the Ho order. This would suggest that the magnetoelectric interaction caused by the Ho moments couples differently to the oxygen cage. Furthermore, if the symmetry due to Mn magnetism is not $P2_1nm$ (e.g., if there is *c*-axis FE polarization), the sensitivity of this reflection to the two distortions is not known.

In other *o*-$RMnO_3$ materials ordering of *R* ions does affect the lattice. For example, the Tb^{3+} moments in $TbMnO_3$ order at 7 K. This transition, while producing only a weak variation in $\boldsymbol{P}$, has an effect on the phonon spectrum [29]. Shimamoto *et al.* [13] have recently shown that *o*-$HoMnO_3$ films can grow as two layers, strained and relaxed. This provides an alternative explanation for our results. An enhancement of the lattice distortion could have also occurred in our samples of *o*-$HoMnO_3$, if we consider the difference in penetration depth for the two diffraction experiments: the RXD experiment probes magnetic order within the first ∼10–20 nm of the film, while the XRD experiment probes the lattice distortion in the entire film. Assuming that only the top of the film is relaxed and bulklike, while the bottom of the film is strained, the T_{Ho1} transition might occur at 14.5 K only in the relaxed part which is probed magnetically by the RXD. To observe an XRD signal originating from an enhanced lattice distortion in these top few nm, it would need to be comparable in magnitude to the existing XRD signal from the whole film. In this case the lattice distortion from T_{Ho1} would most likely not be detected in the XRD experiment in Fig. 6, in contrast to the resonantly enhanced magnetic RXD signals.

V. CONCLUSIONS

Bulklike samples of thick *o*-$HoMnO_3$ films have been studied using x-ray diffraction techniques, sensitive either to the Mn AF order, to Ho AF order, or to the magnetically induced lattice distortion. We observe a series of three magnetic transitions. We find that the Mn AF order is strongly affected by an AF ordering transition of Ho moments at 14.5 K. The same transition is also associated with a strong enhancement of the ferroelectric polarization, but we find no evidence of an enhancement of the lattice distortion associated with the Mn-induced symmetry lowering. Based on our results we suggest that the Ho order that forms below 14.5 K is an *ac* cycloid. Ho m_c moments are known to couple to the Mn order, but the absence of a Ho-ordering signature on the Mn-induced lattice distortion suggests an alternative route to enhanced polarization which is not through Mn.

ACKNOWLEDGMENTS

Experiments were performed at the X11MA and X04SA beamlines at the Swiss Light Source, Paul Scherrer Institute (Villigen, Switzerland). We thank Dr. Y. Hu for sample growth at PSI. We thank the X11MA and X04SA beamline staff for experimental support. The financial support of PSI and the Swiss National Science Foundation (SNSF) is gratefully acknowledged for Y.W.W. through Grants No. 200020-159220 and No. 200021-137657, M.R. through Sinergia Grant No. CRSII2_147606, and L.R. from the SNSF's National Center of Competence in Research Molecular Ultrafast Science and Technology (NCCR MUST), Grant No. 51NF40-183615. We further acknowledge the support of SNSF through Project No. 200020-117642 and through the NCCR MaNEP. This work received funding from the DFG within the Emmy Noether program under Grant No. RE 3977/1.

APPENDIX A

Here we discuss the crystal structure of the films used, and the validity of assuming a good representation of bulk behavior. The lattice constants of the films were estimated in the XRD experiment, and are listed in Table I, alongside bulk values from the literature. This experiment probes the entire film thickness due to the very large penetration depths of the hard x rays. However, the high resonant cross section in the RXD experiment causes a significant reduction in the penetration depth at the resonant energies, meaning that the magnetic properties reported reflect the characteristics of the

TABLE I. Estimated lattice constants of the films used in this work at base temperature. The estimate is an average of the entire film thickness. Corresponding literature values of bulk $HoMnO_3$ and the substrate are also given (units: Å).

Sample	*a*	*b*	*c*
120 nm	5.27	5.78	7.42
240 nm	5.27	5.79	7.39
Bulk *o*−$HoMnO_3$ [6]	5.2481	5.8188	7.3431
$NdGaO_3$	5.43	5.50	7.71

topmost layers of the samples (typically ∼20 nm). Given the low mismatch between the mean film values and bulk values, it is likely that the volume probed in RXD for magnetic properties is fully relaxed. Furthermore, Ref. [13] demonstrated that thick films with higher mismatch already reflect bulk multiferroic properties.

APPENDIX B

The purpose of this Appendix is to gain insight into the sensitivity of the RXD signals to different components of the magnetic moments. To do so, we follow Refs. [30,31] to employ spherical tensor notation. This is not strictly required, but provides a clearer picture of the observations. In this notation a tensor can be written as T_Q^K, in which K is the tensor's rank and Q is its projection. We also limit ourselves to consider dipolar excitations only (E1E1). For a reflection defined by a momentum transfer $\boldsymbol{\tau} = 2\pi(hkl)$, ($hkl$ are miller indices) the resonant structure factor can be written as

$$F(E1, \boldsymbol{\tau}) \propto \sum_{KQ} (-1)^Q \chi_Q^K D_{Qq}^K \Psi_q^K(\boldsymbol{\tau}). \tag{B1}$$

The proportionality term does not concern us in this discussion. Here X_Q^K describes the light, and Ψ_Q^K describes the material (D_{Qq}^K is a rotation of Ψ_q^K to the coordinate system of χ_Q^K). This separation is instrumental, because for understanding the sensitivity of a reflection to specific terms, all that is needed is knowledge of Ψ_q^K. This is described as

$$\Psi_Q^K(\boldsymbol{\tau}) = \sum_d \langle T_Q^K \rangle_d e^{i\boldsymbol{\tau}\cdot\boldsymbol{d}}. \tag{B2}$$

Here T_Q^K is a tensor of rank K describing a component of the electronic cloud (charge, spin, etc …). The brackets denote a time average, and the sum is over all resonant ions in the unit cell. As we concern ourselves only with magnetic dipolar moments, we limit ourselves to a rank of $K = 1$, and thus projections $Q = -1, 0, 1$. To relate Cartesian moments to $\langle T_0^1 \rangle$ objects, one can utilize a simple conversion presented in Ref. [30]: the c axis moment m_c is described by $\langle T_0^1 \rangle$, while the a and b moments are described as $\langle T_{\pm 1}^1 \rangle = (-im_y \mp m_x)/\sqrt{2}$. $\langle T_{\pm 1}^1 \rangle$ are two entities that we will only consider together in this discussion. Alternatively, a more complex object representing a cycloid was used in Ref. [32].

We are now ready to analyze the signals observed. For the Mn ions we use $\boldsymbol{\tau} = 2\pi(0k0)$, since only the $(0\,q\,0)$ reflection is observed. We plug in the Mn ions' $4b$ positions into Eq. (B2), and find that $\Psi_{\pm 1}^1 = 0$, while $\Psi_0^1(\boldsymbol{\tau}) = 2\langle T_0^1 \rangle (1 - e^{\pi i k})$. This reaffirms conclusion of previous works, that the $(0\,q\,0)$ reflection at the Mn edge is sensitive *only* to the c axis moments, i.e., to $\langle T_0^1 \rangle$.

We repeat this for the Ho ions, plugging in their crystallographic $4c$ positions of type $(x\,y\,\frac{1}{4})$, which are described by two free parameters: x and y. For $\boldsymbol{\tau} = 2\pi(0\ k\ 0)$ we find

$$\begin{aligned} \Psi_0^1(0k0) &= -4i\langle T_0^1 \rangle \cos(2\pi yk) \sin\left(\tfrac{1}{2}\pi k\right) e^{(1/2)i\pi k}, \\ \Psi_{\pm 1}^1(0k0) &= 2i \sin(2\pi yk)\left(\langle T_{\pm 1}^1 \rangle + \langle T_{\mp 1}^1 \rangle e^{i\pi k}\right) \end{aligned} \tag{B3}$$

while for $\boldsymbol{\tau} = 2\pi(0\ k\ l)$ we find

$$\begin{aligned} \Psi_0^1(0kl) &= 4\langle T_0^1 \rangle \sin(2\pi yk) \sin\left(\tfrac{1}{2}\pi k\right) e^{1/2i\pi k}, \\ \Psi_{\pm 1}^1(0kl) &= 2\cos(2\pi yk)\left(\langle T_{\pm 1}^1 \rangle + \langle T_{\mp 1}^1 \rangle e^{i\pi k}\right). \end{aligned} \tag{B4}$$

For further insight, we inspect the quantity $\zeta = 2\pi yk$. We plug in $k = q \approx 0.40$ and $y \approx 0.084$ [6,11], and find that $\cos\zeta \approx 1$ while $\sin\zeta \approx 0.2$. This implies that $(0\,q\,0)$ at the Ho edge is primarily sensitive to $\langle T_0^1 \rangle$ and weakly sensitive to $\langle T_{\pm 1}^1 \rangle$, unlike the Mn resonance, in which sensitivity is *only* to $\langle T_0^1 \rangle$. For $(0\,q\,1)$ the opposite is true: it is strongly sensitive to $\langle T_{\pm 1}^1 \rangle$ and weakly sensitive to $\langle T_0^1 \rangle$. From these conclusions we conclude that $(0\,q\,1)$ is primarily sensitive to the Ho m_{ab} and $(0\,q\,0)$ is primarily sensitive to m_c.

[1] S. Ishiwata, Y. Kaneko, Y. Tokunaga, Y. Taguchi, T. H. Arima, and Y. Tokura, Perovskite manganites hosting versatile multiferroic phases with symmetric and antisymmetric exchange strictions, Phys. Rev. B **81**, 100411(R) (2010).

[2] M. Kenzelmann, A. B. Harris, S. Jonas, C. Broholm, J. Schefer, S. B. Kim, C. L. Zhang, S.-W. Cheong, O. Vajk, and J. W. Lynn, Magnetic Inversion Symmetry Breaking and Ferroelectricity in $TbMnO_3$, Phys. Rev. Lett. **95**, 087206 (2005).

[3] H. Okamoto, N. Imamura, B. Hauback, M. Karppinen, H. Yamauchib, and H. Fjellvåg, Neutron powder diffraction study of crystal and magnetic structures of orthorhombic $LuMnO_3$, Solid State Commun. **146**, 152 (2008).

[4] M. Mochizuki and N. Furukawa, Microscopic model and phase diagrams of the multiferroic perovskite manganites, Phys. Rev. B **80**, 134416 (2009).

[5] M. Mochizuki, N. Furukawa, and N. Nagaosa, Theory of spin-phonon coupling in multiferroic manganese perovskites $R MnO_3$, Phys. Rev. B **84**, 144409 (2011).

[6] H. W. Brinks, J. Rodríguez-Carvajal, H. Fjellvåg, A. Kjekshus, and B. C. Hauback, Crystal and magnetic structure of orthorhombic $HoMnO_3$, Phys. Rev. B **63**, 094411 (2001).

[7] O. Prokhnenko, R. Feyerherm, E. Dudzik, S. Landsgesell, N. Aliouane, L. C. Chapon, and D. N. Argyriou, Enhanced Ferroelectric Polarization by Induced Dy Spin Order in Multiferroic $DyMnO_3$, Phys. Rev. Lett. **98**, 057206 (2007).

[8] T. Kimura, G. Lawes, T. Goto, Y. Tokura, and A. Ramirez, Magnetoelectric phase diagrams of orthorhombic $R MnO_3$ (R = Gd, Tb, and Dy), Phys. Rev. B **71**, 224425 (2005).

[9] N. Lee, Y. J. Choi, M. Ramazanoglu, W. Ratcliff, II, V. Kiryukhin, and S.-W. Cheong, Mechanism of exchange striction of ferroelectricity in multiferroic orthorhombic $HoMnO_3$ single crystals, Phys. Rev. B **84**, 020101(R) (2011).

[10] B. Lorenz, Y.-Q. Wang, and C.-W. Chu, Ferroelectricity in perovskite $HoMnO_3$ and $YMnO_3$, Phys. Rev. B **76**, 104405 (2007).

[11] A. Muñoz, M. T. Casais, J. A. Alonso, M. J. Martinez-Lope, M. M. T, and J. L. Fernez-Diaz, Complex magnetism and magnetic structures of the metastable $HoMnO_3$ perovskite, Inorg. Chem. **40**, 1020 (2001).

[12] T. Kimura, S. Ishihara, H. Shintani, T. Arima, K. T. Takahashi, K. Ishizaka, and Y. Tokura, Distorted perovskite with eg 1 configuration as a frustrated spin system, Phys. Rev. B **68**, 060403(R) (2003).

[13] K. Shimamoto, Y. W. Windsor, Y. Hu, M. Ramakrishnan, A. Alberca, E. M. Bothschafter, L. Rettig, T. Lippert, U. Staub, and C. W. Schneider, Multiferroic properties of uniaxially compressed orthorhombic $HoMnO_3$ thin films, Appl. Phys. Lett. **108**, 112904 (2016).

[14] U. Staub, V. Scagnoli, Y. Bodenthin, M. García-Fernández, R. Wetter, A. Mulders, H. Grimmer, and A. M. Horisberger, Polarization analysis in soft X-ray diffraction to study magnetic and orbital ordering, J. Synchrotron Radiat. **15**, 469 (2008).

[15] U. Fleschig, F. Nolting, A. Fraile Rodríguez, J. Krempaský, C. Quitmann, T. Schmidt, S. Spielmann, and D. Zimoch, Performance measurements at the SLS SIM beamline, in *SRI 2009, 10th International Conference on Radiation Instrumentation*, edited by R. Garrett, I. Gentle, K. Nugent, and S. Wilkins, AIP Conf. Proc. No. 1234 (AIP, New York, 2010), p. 319, https://doi.org/10.1063/1.3463200.

[16] R. Willmott, The materials science beamline upgrade at the swiss light source, J. Synchrotron Radiat. **20**, 667 (2013).

[17] C. Broennimann, E. F. Eikenberry, B. Henrich, R. Horisberger, G. Huelsen, E. Pohl, B. Schmitt, C. Schulze-Briese, M. Suzuki, T. Tomizaki, H. Toyokawa, and A. Wagner, The PILATUS 1M detector, J. Synchrotron Radiat. **13**, 120 (2006).

[18] M. Garganourakis, Y. Bodenthin, R. A. D. Souza, V. Scagnoli, A. Dönni, M. Tachibana, H. Kitazawa, E. Takayama-Muromachi, and U. Staub, Magnetic and electronic orderings in orthorhombic $R MnO_3$ (R = Tm, Lu) studied by resonant soft x-ray powder diffraction, Phys. Rev. B **86**, 054425 (2012).

[19] Y. W. Windsor, M. Ramakrishnan, L. Rettig, A. Alberca, E. M. Bothschafter, U. Staub, K. Shimamoto, Y. Hu, T. Lippert, and C. W. Schneider, Interplay between magnetic order at Mn and Tm sites alongside the structural distortion in multiferroic films of o-$TmMnO_3$, Phys. Rev. B **91**, 235144 (2015).

[20] N. Aliouane, O. Prokhnenko, R. Feyerherm, M. Mostovoy, J. Strempfer, K. Habicht, K. C. Rule, E. Dudzik, A. U. B. Wolter, A. Maljuk, and D. N. Argyriou, Magnetic order and ferroelectricity in $R MnO_3$ multiferroic manganites: Coupling between R- and Mn-spins, J. Phys.: Condens. Matter **20**, 434215 (2008).

[21] Y. W. Windsor, S. W. Huang, Y. Hu, L. Rettig, A. Alberca, K. Shimamoto, V. Scagnoli, T. Lippert, C. W. Schneider, and U. Staub, Multiferroic Properties of o-$LuMnO_3$ Controlled by B-Axis Strain, Phys. Rev. Lett. **113**, 167202 (2014).

[22] J. P. Hill and D. F. McMorrow, X-ray resonant exchange scattering: polarization dependence and correlation functions, Acta Crystallogr., Sect. A **52**, 236 (1996).

[23] H. Wadati, J. Okamoto, M. Garganourakis, V. Scagnoli, U. Staub, Y. Yamasaki, H. Nakao, Y. Murakami, M. Mochizuki, M. Nakamura, M. Kawasaki, and Y. Tokura, Origin of the Large Polarization in Multiferroic $YMnO_3$ Thin Films Revealed by Soft- and Hard-X-Ray Diffraction, Phys. Rev. Lett. **108**, 047203 (2012).

[24] D. Okuyama, S. Ishiwata, Y. Takahashi, K. Yamauchi, S. Picozzi, K. Sugimoto, H. Sakai, M. Takata, R. Shimano, Y. Taguchi, T. Arima, and Y. Tokura, Magnetically driven ferroelectric atomic displacements in orthorhombic $YMnO_3$, Phys. Rev. B **84**, 054440 (2011).

[25] V. Scagnoli, U. Staub, Y. Bodenthin, M. García-Fernández, A. M. Mulders, and G. I. M. G. Hammerl, Induced noncollinear magnetic order of Nd3+ in $NdNiO_3$ observed by resonant soft x-ray diffraction, Phys. Rev. B **77**, 115138 (2008).

[26] S. Mukherjee, S. K., C. W. Schneider, and C. Niedermayer, Unique coexistence of incommensurate and commensurate magnetic order in $TbMnO_3$ strained films, Phys. Rev. Materials **3**, 104412 (2019).

[27] J. Voigt, J. Perrson, J. W. Kim, G. Bihlmayer, and T. Brückel, Strong coupling between the spin polarization of Mn and Tb in multiferroic $TbMnO_3$ determined by X-ray resonance exchange scattering, Phys. Rev. B **76**, 104431 (2007).

[28] D. Mannix, D. F. McMorrow, R. A. Ewings, A. T. Boothroyd, D. Prabhakaran, Y. Joly, B. Janousova, C. Mazzoli, L. Paolasini, and S. B. Wilkins, X-ray scattering study of the order parameters in multiferroic $TbMnO_3$, Phys. Rev. B **76**, 184420 (2007).

[29] R. Schleck, R. L. Moreira, H. Sakata, and R. S. M. Lobo, Infrared reflectivity of the phonon spectra in multiferroic $TbMnO_3$, Phys. Rev. B **82**, 144309 (2010).

[30] S. Lovesey, E. Balcar, K. Knight, and J. Fernández Rodríguez, Electronic properties of crystalline materials observed in X-ray diffraction, Phys. Rep. **411**, 233 (2005).

[31] V. Scagnoli, Ph.D. thesis, Electronic and magnetic ordering phenomena at metal-insulator transitions probed by resonant X-ray scattering, ETH, Zürich, 2005, https://doi.org/10.3929/ethz-a-005133594.

[32] S. Lovesey, V. Scagnoli, M. Garganourakis, S. M. Koohpayeh, C. Detlefs, and U. Staub, Melting of chiral order in terbium manganate ($TbMnO_3$) observed with resonant x-ray Bragg diffraction, J. Phys.: Condens. Matter **25**, 362202 (2013).